Assessing the Influence of Secondary Organic versus Primary Carbonaceous Aerosols on Long-Range Atmospheric Polycyclic Aromatic Hydrocarbon Transport*

C.L. Friedman, J.R. Pierce and N.E. Selin

MIT JOINT PROGRAM ON THE SCIENCE AND POLICY of GLOBAL CHANGE

***Reprinted from**
***Environmental Science & Technology*, 48(6): 3293–3302**

Reprint 2014-5

The MIT Joint Program on the Science and Policy of Global Change combines cutting-edge scientific research with independent policy analysis to provide a solid foundation for the public and private decisions needed to mitigate and adapt to unavoidable global environmental changes. Being data-driven, the Program uses extensive Earth system and economic data and models to produce quantitative analysis and predictions of the risks of climate change and the challenges of limiting human influence on the environment—essential knowledge for the international dialogue toward a global response to climate change.

To this end, the Program brings together an interdisciplinary group from two established MIT research centers: the Center for Global Change Science (CGCS) and the Center for Energy and Environmental Policy Research (CEEPR). These two centers—along with collaborators from the Marine Biology Laboratory (MBL) at Woods Hole and short- and long-term visitors—provide the united vision needed to solve global challenges.

At the heart of much of the Program's work lies MIT's Integrated Global System Model. Through this integrated model, the Program seeks to: discover new interactions among natural and human climate system components; objectively assess uncertainty in economic and climate projections; critically and quantitatively analyze environmental management and policy proposals; understand complex connections among the many forces that will shape our future; and improve methods to model, monitor and verify greenhouse gas emissions and climatic impacts.

This reprint is one of a series intended to communicate research results and improve public understanding of global environment and energy challenges, thereby contributing to informed debate about climate change and the economic and social implications of policy alternatives.

Ronald G. Prinn and John M. Reilly,
Program Co-Directors

For more information, contact the Program office:
MIT Joint Program on the Science and Policy of Global Change

Postal Address:
Massachusetts Institute of Technology
77 Massachusetts Avenue, E19-411
Cambridge, MA 02139 (USA)

Location:
Building E19, Room 411
400 Main Street, Cambridge

Access:
Tel: (617) 253-7492
Fax: (617) 253-9845
Email: ***globalchange@mit.edu***
Website: ***http://globalchange.mit.edu/***

Environmental Science & Technology

Article

pubs.acs.org/est

Assessing the Influence of Secondary Organic versus Primary Carbonaceous Aerosols on Long-Range Atmospheric Polycyclic Aromatic Hydrocarbon Transport

C. L. Friedman,*[,†] J. R. Pierce,[§] and N. E. Selin[‡]

[†]Center for Global Change Science and Leading Technology and Policy Initiative and [‡]Engineering Systems Division and Department of Earth, Atmospheric, and Planetary Science, Massachusetts Institute of Technology, Cambridge, Massachusetts 02139, United States

[§]Department of Atmospheric Science, Colorado State University, Fort Collins, Colorado 80523, United States

Supporting Information

ABSTRACT: We use the chemical transport model GEOS-Chem to evaluate the hypothesis that atmospheric polycyclic aromatic hydrocarbons (PAHs) are trapped in secondary organic aerosol (SOA) as it forms. We test the ability of three different partitioning configurations within the model to reproduce observed total concentrations in the midlatitudes and the Arctic as well as midlatitude gas−particle phase distributions. The configurations tested are (1) the GEOS-Chem default configuration, which uses instantaneous equilibrium partitioning to divide PAHs among the gas phase, a primary organic matter (OM) phase (absorptive), and a black carbon (BC) phase (adsorptive), (2) an SOA configuration in which PAHs are trapped in SOA when emitted and slowly evaporate from SOA thereafter, and (3) a configuration in which PAHs are trapped in primary OM/BC upon emission and subsequently slowly evaporate. We also test the influence of changing the fraction of PAHs available for particle-phase oxidation. Trapping PAHs in SOA particles upon formation and protecting against particle-phase oxidation (2) better simulates observed remote concentrations compared to our default configuration (1). However, simulating adsorptive partitioning to BC is required to reproduce the magnitude and seasonal pattern of gas−particle phase distributions. Thus, the last configuration (3) results in the best agreement between observed and simulated concentration/phase distribution data. The importance of BC rather than SOA to PAH transport is consistent with strong observational evidence that PAHs and BC are coemitted.

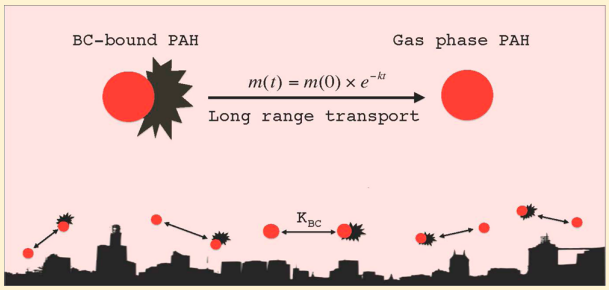

INTRODUCTION

Polycyclic aromatic hydrocarbons (PAHs) are toxic semivolatile organic compounds (SVOCs) that partition between gas and aerosol phases and travel long distances in the atmosphere.[1,2] The chemical and physical processes influencing transport of PAHs from areas of high emissions to remote regions are still largely unknown. In particular, the influence of atmospheric aerosols (i.e., particles) on PAH long-range transport (LRT) is highly uncertain. A number of schemes have been proposed to estimate gas−particle distribution of PAHs, with each predicting different PAH LRT potential. Additionally, there is debate within the atmospheric chemistry literature regarding aerosol formation and evolution over time and how best to simulate these processes. Here, we conduct simulations of atmospheric PAH transport using the chemical transport model GEOS-Chem with different assumptions about (1) gas−particle partitioning and (2) physicochemical characteristics of different aerosol types to test how these variables affect PAH LRT efficiency.

PAHs have been extensively measured in both gas and particle phases. Schemes for estimating measured phase distributions have evolved over time, as recently reviewed by Lohmann and Lammel[3] and Keyte et al.[4] To summarize, PAH gas−particle partitioning has been described with four different schemes, each assuming instantaneous equilibrium partitioning (EqP): (1) the Junge−Pankow adsorption scheme,[5−8] in which PAH adsorption to total suspended particles depends on the PAH subcooled liquid vapor pressure, (2) the Finizio scheme,[9] which partitions PAHs to particles on the basis of a gas−particle equilibrium partition coefficient (K_P = $[PAH]_{particle}/[PAH]_{gas}$) that is empirically related to the octanol−air partition coefficient (K_{OA} = $[PAH]_{octanol}/[PAH]_{air}$), (3) the Harner−Bidleman scheme,[10] which augments the Finizio scheme by accounting for the fraction of organic material (OM; used here interchangeably with "organic aerosol", or OA) within a particle, and finally (4) the Dachs and Eisenreich (D&E) scheme,[11] which considers both absorption into OM

Received: November 22, 2013
Revised: February 6, 2014
Accepted: February 24, 2014
Published: February 24, 2014

and adsorption to black/elemental carbon (BC) within the particle.

In general, the Junge−Pankow, Finizio, and Harner−Bidleman schemes underestimate particulate fractions and particle-phase concentrations (i.e., they underpredict K_P), both when compared directly to observations[3,12,13] and when employed in atmospheric transport models.[14,15] Schemes considering absorption into OM generally perform better than the Junge−Pankow scheme, however. The D&E scheme better represents observed PAH concentrations and phase distributions in various comparisons,[3,12,14−16] especially in remote regions. This is consistent with knowledge about PAH partitioning in the marine environment, where sorption to sedimentary BC limits aquatic PAH concentrations and thus availability and toxicity to marine organisms.[17−20] However, the D&E scheme cannot explain the observed lack of correlation between particle and gas phases[21] and can overpredict observed K_P values.[11] Collectively, the inability of these partitioning schemes to accurately estimate PAH phase distribution suggests the assumption of instantaneous equilibrium is inaccurate.

It has recently been suggested, on the basis of laboratory studies, that PAHs become trapped in secondary organic aerosol (SOA) during SOA formation, preventing them from evaporating to the gas phase and protecting them from degradation via oxidation.[22] This process could explain the observed lack of gas−particle correlation and generally low estimated K_P values compared to measurements. Unlike primary organic aerosol (POA), which is directly emitted to the atmosphere, SOA forms within the atmosphere. Thus, total atmospheric organic aerosol (OA or OM) contains both POA and SOA. SOA has traditionally been considered aerosol formed from the oxidation and condensation of gas-phase precursors, including SVOCs such as PAHs. Recently, however, oxidation of gas-phase compounds that have evaporated from POA has been recognized as another source of SOA.[23] SOA is estimated to comprise over 30% of total atmospheric OM,[24] though this fraction may be much greater if current estimates are missing key sources. The contribution of PAHs to SOA formation could be significant in anthropogenically influenced locations. One study estimated that PAHs account for >10% of SOA in Houston, TX,[25] and another showed that alkanes and PAHs combined may account for 20−30% of ground-level anthropogenic SOA in the United States.[26]

While PAH modeling studies use various schemes for representing gas−particle partitioning, none explicitly consider the role of SOA on PAH LRT. Evaluating the impact of SOA on PAHs is important from two different perspectives. First, if PAHs are trapped in SOA during SOA formation, they may be shielded from oxidative degradation and prevented from exchanging with the gas phase. This could explain why PAH K_P values are generally underpredicted by EqP schemes. Second, OA models, including the GEOS-Chem model used in the present study, tend to underestimate observed OA concentrations, implying potential missing SOA sources.[24] Incorporation of PAHs during SOA formation has been found to significantly decrease SOA evaporation rates,[22] potentially increasing SOA atmospheric lifetimes and simulated OA concentrations, though we do not evaluate this.

Here, we use a global model to test the importance of SOA to PAH LRT, with the hypothesis that incorporating SOA into the model will better reproduce observed gas−particle distributions compared to a model that uses primary carbonaceous aerosols for partitioning. We modify the previously developed and evaluated GEOS-Chem PAH model[27] to include SOA partitioning and compare results from the SOA-inclusive simulation to those from the default simulation, which employs the D&E OM/BC absorption/adsorption EqP scheme. We conduct additional sensitivity simulations to determine the importance of different PAH−aerosol assumptions besides partitioning: aerosol deposition efficiencies, concentrations of primary aerosols (OM/BC) versus SOA, and constant versus spatiotemporally varying oxidant concentrations. We conduct all simulations for pyrene, given its semivolatility (i.e., substantial mass is found in both the gas and particle phases) and because its physicochemical relationship with SOA has been evaluated extensively compared to those of other PAHs.[22]

METHODS

GEOS-Chem PAH Model: Default Configuration. The development and evaluation of the GEOS-Chem PAH model (v8-03-02) have been described in full elsewhere.[27] To summarize, the model includes oxidation of gas-phase PAHs by hydroxyl radical (OH; scaled for diurnal variation), oxidation of particle-phase PAHs by ozone (O_3), wet and dry deposition of both gas- and particle-phase PAHs, and temperature-dependent partitioning between the gas phase and two particle phases (hydrophobic primary OM and BC) following the D&E scheme.[11] The particle phases used in the default model are primary hydrophobic carbonaceous aerosols only; i.e., "primary OM" refers to OM that does not include SOA. K_{OA} values are used to describe absorptive partitioning between the gas and primary OM phases, and BC−air equilibrium partition coefficients ($K_{BC} = [PAH]_{BC}/[PAH]_{gas}$) describe adsorptive partitioning between gas and BC. A separate NO_x−O_x−hydrocarbon−aerosol version of GEOS-Chem (v9-01-02) is used to generate monthly mean concentrations of OH, O_3, hydrophobic organic carbon (OC), and hydrophobic BC, which are archived and read into the PAH model as input. Sensitivity simulations with daily versus monthly oxidant and aerosol inputs suggest monthly averaging results in, at most, a 2% change in PAH concentrations.[28] OC concentrations are multiplied by 1.8 to represent primary OM.[29] OM and BC particles with which PAHs are associated convert from hydrophobic to hydrophilic species with a lifetime of 1.2 days,[30] increasing the efficiency of wet scavenging over time with no change in PAH chemistry. PAHs partition between the gas phase and hydrophobic aerosols only; once particles become hydrophilic, PAHs remain associated with the particle until depositing. In the default model, BC plays a much larger role than primary OM in sequestering PAHs within the particle phase: 98% of particulate PAHs are associated with BC rather than OM. A land−atmosphere exchange module was developed and employed recently to evaluate the effect of climate on PAH transport;[28] to reduce variables in the present study, however, we neglect land−atmosphere exchange, which results in minor (∼1%) decreases to simulated concentrations with no effect on partitioning. We use a global PAH primary emissions inventory from 2004 compiled on a country-by-country basis, spatially allocated on a 1° × 1° grid,[31] and assimilated meteorology from the NASA Goddard Earth Observing System's GEOS5 data set degraded to 6 h temporally, 4° × 5° horizontally, and 47 levels vertically. All physicochemical constants used are shown in Table S1 (Supporting Information). We refer to our standard PAH model using the D&E partitioning scheme as the "default" configuration.

Table 1. Summary of Simulations Conducted in This Study

Simulation	Model configuration	Emission scenario	Instantaneous EqP?	% of PAH available for particle-phase oxidation	Additional details	Color in figures
			1. SIMULATIONS TO EVALUATE PARTITIONING			
1a	Default	OM, BC, and gas	Yes	0%		
1b	Default	OM, BC, and gas	Yes	100%		
1c	SOA-PAH	100% in SOA	No	0%		
1d	SOA-PAH	100% in SOA	No	10%		
1e	SOA-PAH	SOA/gas	No	0%		
1f	SOA-PAH	SOA/gas	No	10%		
			2. SIMULATIONS TO EVALUATE SENSITIVITY TO OTHER MODEL PARAMETERS			
2a*	SOA-PAH	100% in SOA	No	0%	OM/BC wet deposition efficiency substituted for SOA	
2b*	SOA-PAH	SOA/gas	No	0%	Constant OH concentration	
2c	SOA-PAH	SOA/gas	No	0%	Sum of OM/BC concentrations in place of SOA concentrations	
			3. SIMULATIONS TO EVALUATE THE ROLE OF INSTANTANEOUS EQUILIBRIUM PARTITIONING VERSUS AEROSOL TYPE			
3a	OM/BC-evap	OM, BC, and gas	No	0%	Default model without equilibrium partitioning	
3b	OM/BC-evap	OM, BC, and gas	No	10%	Default model without equilibrium partitioning	

[a]An asterisk indicates the simulation results are presented in the Supporting Information.

Default Configuration Updates and Modifications. The version of the model used here includes several updates relative to previously published work.[27,28] We include particle-phase oxidation by NO_3 (in addition to O_3) following recently published data.[32] We use monthly mean NO_3 concentrations archived from NO_x–O_x–hydrocarbon–aerosol GEOS-Chem simulations, scaled for diurnal variation, and reaction rates provided by Liu et al.[32] (Table S1, Supporting Information). We also use improved leaf area indices (LAIs) for calculating dry deposition fluxes. We evaluate the influence of including these processes on simulated PAH concentrations relative to previous model versions in the Supporting Information (Figures S1 and S2); in general, these updates improve model–measurement comparisons.

SOA–PAH Configuration. We develop a separate configuration of the GEOS-Chem PAH model to address SOA partitioning (the "SOA–PAH" configuration). We first generate global SOA concentrations with the GEOS-Chem NO_x–O_x–hydrocarbon–aerosol model (v9-01-02).[33] GEOS-Chem assumes sources of 23.4 Tg yr^{-1} biogenic and 3.1 Tg yr^{-1} anthropogenic SOA, the combination of which is on the low end of SOA estimates.[24] This does not include a ~100 Tg yr^{-1} source of "anthropogenically enhanced" SOA that has been recommended for inclusion in models on the basis of reduced mean error between simulated SOA concentrations and measurements,[34,35] and we discuss uncertainties associated with this below. We archive monthly mean concentrations of total SOA (mean of 2006–2008) for input to the PAH model. Simulated SOA surface concentrations are generally several times greater than primary hydrophobic OM and BC concentrations (Figure S3, Supporting Information). For the SOA–PAH configuration, we simulate PAHs in two phases: a gas phase and a particle phase consisting solely of SOA-bound PAHs (ignoring partitioning to primary OM and BC). Gas-phase PAHs oxidize and deposit as described above and in our previous PAH model studies.[27,28] SOA-bound PAHs are scavenged in convective updrafts, rainout, and washout with an efficiency of 80% as described by Chung and Seinfeld,[36] consistent with SOA behavior in GEOS-Chem.[24,33] This differs from the behavior of primary OM- and BC-bound PAHs in the default simulation, which are wet scavenged at 0% efficiency while hydrophobic and 100% efficiency after becoming hydrophilic. Dry deposition is treated similarly to the default simulation, following a resistance-in-series scheme[37] with no size dependence.

Simulations To Evaluate Partitioning. We use the default and SOA–PAH configurations described above to run individual simulations comparing the effect of these different partitioning schemes on PAH LRT. Table 1 lists these simulations in section 1, with additional sensitivity simulations (discussed below) in section 2. Simulations employing the SOA–PAH configuration are divided into two emissions scenarios on the basis of uncertainties in phase distribution upon emission. In the default configuration, PAHs are emitted as total mass (gas plus particle) and distributed instantaneously between the gas and primary OM/BC phases according to K_{OA}, K_{BC}, and ambient OM/BC concentrations within the boundary layer. This is a known source of uncertainty, as in situ measurements of the phase upon emission are limited or vary substantially for most major PAH sources. Similarly, few data exist to suggest a suitable approach for distributing emissions between gas and SOA phases. Thus, we construct two emissions scenarios within the SOA–PAH configuration to capture a range of potential phase distributions upon emission: (a) 100% of PAHs are trapped in SOA upon emission (denoted "100% in SOA"), and (b) the fraction of PAH emissions trapped is determined by partitioning between SOA and gas phases according to K_{OA} and boundary layer SOA concentrations ("SOA/gas"). Both scenarios assume PAHs can only become trapped in SOA within the 4° × 5° grid box into which PAHs are emitted. Though both scenarios may neglect entrapment after LRT, the lifetimes of SOA precursors are short enough that SOA formation relevant to PAH entrapment likely happens before substantial LRT has taken place; i.e., we assume the effect is small.

After initial partitioning as described above, simulations employing the SOA–PAH configuration use a chemistry and partitioning scheme following the experimental results of Zelenyuk et al.[22] In contrast to the instantaneous EqP scheme of the default configuration, PAHs in SOA–PAH simulations slowly evaporate from SOA after their initial entrapment. According to Zelenyuk et al., ~50–80% of PAHs trapped in SOA during SOA formation remain associated with the particle after 24 h, with 80% likely the more realistic estimate given differences between laboratory and atmospheric conditions. We

model this evaporation process using an exponential decay function:

$$m(t) = m(0)\, e^{-kt} \quad (1)$$

where $m(t)$ is the mass of SOA-bound PAHs at time t, $m(0)$ is the initial mass of SOA-bound PAHs, and k is the evaporation rate, which is set to correspond to 80% PAHs remaining after 24 h (unless otherwise noted). Zelenyuk et al. also estimated that only 10% of PAHs associated with SOA are on or near the particle surface. We thus assume for SOA−PAH simulations that only 10% of SOA-associated PAHs are susceptible to heterogeneous particle-phase oxidation, in contrast to the default configuration where 100% of primary OM and BC-associated PAHs undergo oxidation. For both the default and SOA−PAH configurations, we conduct simulations with and without particle-phase oxidation, and SOA−PAH simulations are conducted under both emissions scenarios (simulations 1a−1f in section 1 in Table 1).

We note that there are several uncertainties associated with the Zelenyuk scheme that have implications for results from SOA−PAH simulations, including the degree to which SOA exists as a viscous, semisolid substance in the atmosphere, which namely depends on the temperature and relative humidity[38] (Zelenyuk et al. conducted their experiments under dry conditions). These uncertainties could modify the degree of PAH trapping and oxidation and lead to variations in resulting gas/particle ratios. We address this by running simulations with an evaporation rate corresponding to 50% PAHs remaining trapped after 24 h, the lower limit of the range mentioned above.

Simulations To Evaluate Sensitivity to Other Model Parameters. We conduct three additional sensitivity simulations with the SOA−PAH configuration to test the influence of parameters not directly related to the partitioning scheme (simulations 2a−2c, Table 1). These are: differences in wet deposition efficiency between primary OM/BC and SOA, the influence of OH concentration, and the concentration/spatiotemporal difference between OM/BC and SOA. To test the effect of differences in wet deposition efficiency, which could affect particulate PAH lifetimes relevant to LRT, we replace the deposition efficiency of SOA with that of hydrophobic OM/BC (simulation 2a, Table 1). OH concentrations influence gas-phase degradation lifetimes. Some previous PAH modeling exercises have assumed constant OH concentrations,[22] while others have found that seasonal variations in OH can cause marked differences in PAH concentrations.[39] To diagnose the influence of these assumptions, we replace spatially and temporally varying OH concentrations with a blanket OH concentration of 10^6 molecules/cm^3 (simulation 2b). Spatial and temporal variability in aerosols could also affect transport pathways by changing particle availability for partitioning and thus PAH gas−particle distribution. To assess differences in the spatial and temporal distribution of hydrophobic primary aerosols versus SOA, we use monthly mean archived concentrations of primary OM/BC in place of SOA concentrations (simulation 2c).

The "100% in SOA" emissions scenario is more sensitive than the "SOA/gas" scenario to the effect of wet deposition, since it allocates a greater fraction of PAHs (100%) to the particulate phase, while the SOA/gas emissions scenario has greater sensitivity to spatial and temporal distribution of aerosol. The latter is because when PAHs are divided between gas and particulate phases by K_{OA}, the fraction of particulate PAHs is calculated according to the volume ratio between air and particles; hence, particle concentrations need to be known. This is in contrast to the 100% in SOA emissions scenario, where there is no dependence on particle concentration because the PAH particulate fraction is assumed to be independent of air/particle volume ratios. Finally, the SOA/gas emissions scenario is more sensitive to changes in OH, because a greater fraction of PAHs exist in the gas phase. We thus use the 100% in SOA scenario for our wet deposition sensitivity simulations and the SOA−gas partitioning emissions scenario for spatial and temporal distribution and OH sensitivity simulations. Partitioning in the latter two sensitivity scenarios follows the SOA/gas emissions scenario using the K_{OA} alone to partition PAHs upon emission, even when primary OM/BC is substituted for SOA (i.e., the K_{BC} is not used, so we can isolate the effect of aerosol concentration/deposition versus difference in partitioning strength).

Simulations To Assess the Role of Instantaneous Equilibrium Partitioning versus Aerosol Type: OM/BC-evap Configuration. In a final set of simulations (Table 1, section 3), we evaluate the possibility that PAHs are trapped in primary carbonaceous species (OM/BC) rather than SOA, with subsequent slow evaporation following eq 1 as in the SOA−PAH configuration. In this configuration, termed "OM/BC-evap", PAHs partition to ambient primary OM/BC when emitted following both K_{OA} and K_{BC}, and 80% of PAHs remain in the particle after 24 h. The OM/BC-evap configuration isolates the effect of SOA versus BC (i.e., aerosol type) from the effect of EqP because (1) the trapping scenario is used instead of EqP and (2) in all simulations where primary OM and BC represent the particle phase, BC-bound PAHs account for 98% of the particle-phase budget; primary OM plays only a minor role in sequestering pyrene. We conduct simulations with this "OM/BC-evap" configuration with and without particle-phase oxidation (simulations 3a and 3b, Table 1).

Model Evaluation. To evaluate how well each simulation captures observed concentrations, we conduct paired t tests for differences between simulated and observed three-year (2006−2008) mean total (gas + particulate) concentrations at northern hemisphere stations reporting at least monthly measurements (see Table S2 (Supporting Information) for station information). We compare annual means only at stations distant from sources (i.e., nonurban midlatitude and Arctic sites). We also compare simulated and observed monthly mean total concentrations from sites in Table S2 to assess how well simulations capture seasonal variability at nonurban midlatitude and Arctic sites. Finally, we compare simulated and observed monthly mean particulate fractions (i.e., $[PAH]_{particulate}/[PAH]_{total}$). We make this comparison only at stations operated by the Integrated Atmospheric Deposition Network (IADN; over the U.S. and Canadian Great Lakes), where phase-resolved measurements are prioritized and considered reliable for model evaluation.

RESULTS

Statistical Comparison of Annual Means. Scatter plots of simulated versus observed mean concentrations are shown in Figure S4 (Supporting Information), while linear best fit equations, correlation coefficients (r = 0.65−0.70), and log mean biases (LMB = −0.08−0.21) are shown in Table S3 (Supporting Information). Our default configuration is able to capture annual mean PAH concentrations: for default simulations (1a and 1b, Table 1), there is no significant

difference (α = 0.05) between simulated and observed annual means, both with and without particle-phase oxidation turned on (p = 0.97 and 0.07, respectively). Annual means from SOA–PAH simulations using the SOA/gas emissions scenario (1e and 1f) also are not statistically different from observed means (p = 0.27 and 0.26 for with and without particle-phase oxidation, respectively). In contrast, comparison of simulated and observed annual means shows that simulating 100% PAH entrapment in SOA upon emission does not match observations of LRT (1c and 1d). Annual means are significantly higher than observations for SOA–PAH simulations when 100% of emissions are allocated to SOA: simulated concentrations are 4.4× higher than observed with particle-phase oxidation (p = 0.01) and 7.4× higher without (p < 0.01). These results confirm that if PAHs are indeed trapped in SOA upon emission, it is unlikely that 100% of PAHs become associated with SOA.

SOA–PAH simulations using an evaporation rate corresponding to 50% of particulate PAHs remaining after 24 h (rather than the default of 80%) resulted in, at most, a 15% decrease in simulated annual mean concentrations (data not shown). Though this is a relatively minor change, we note that the 50–80% evaporation rate range used here was obtained under dry conditions, which are unlikely in the atmosphere. Thus, true atmospheric evaporation rates probably have even greater variability and could have a stronger influence on PAH concentrations.

Monthly Mean Concentrations. We compare monthly mean observed and simulated total concentrations and particulate fractions to further assess simulations using different partitioning schemes (in section 1 in Table 1). Parts A and B of Figure 1 show simulated vs observed monthly means at nonurban midlatitude and Arctic stations, respectively, while part C compares simulated and observed particulate fractions at IADN sites over the U.S./Canadian Great Lakes. Results from simulations to evaluate partitioning (Table 1, 1a–1f; green, blue, and red lines in Figure 1) are compared to observations (black lines) in this section; simulations to evaluate the effect of PAH trapping by BC (Table 1, 3a and 3b; purple lines in Figure 1) are discussed later.

Comparison of simulated and observed monthly midlatitude concentrations (Figure 1A) shows that phase distribution upon emission has more influence on PAH LRT than partitioning behavior during transport. All simulations capture the intermonthly trend in midlatitude concentrations (more in winter, less in summer). Simulations in which PAHs are partitioned between gas and particle phases upon emission (1a, 1b, 1e, and 1f, Table 1; green and red lines, Figure 1A) result in concentrations that fall within ± 1 standard deviation of monthly means, regardless of whether they are partitioned to primary OM/BC or SOA and whether they follow the default EqP scheme or the SOA–PAH scheme. Consistent with the annual mean comparison, SOA–PAH simulations following the 100% in SOA emissions scenario (1c and 1d, Table 1; blue lines, Figure 1A) overestimate measured values. Including particle-phase oxidation (dotted lines) does not substantially change the results.

In contrast to midlatitude concentrations, comparisons to monthly mean Arctic concentrations (Figure 1B) show that when larger fractions of PAHs are distributed to the particle phase upon emission and protected from oxidation, there is a better match to observations. All simulations generally capture concentrations during colder months within ±1 standard deviation of measured means, but underestimate summer concentrations by up to ~100-fold. Summer underestimates are likely partially due to the influence of local sources not included in model emissions (e.g., camp- or wildfires).[40] Simulated concentrations are generally higher, and closer to Arctic measured values, when a greater fraction of PAHs are allocated to the particle phase when emitted and protected from oxidation. Thus, in contrast to annual mean and midlatitude monthly comparisons, the SOA–PAH 100% in SOA scenario performs best, consistent with the hypothesis that trapping of PAHs in SOA may account for high particulate fractions in remote areas.[22] Similar to the midlatitudes, however, simulated transport to the Arctic is more strongly influenced by distribution upon emission than the partitioning scheme subsequent to emission; e.g., simulations 1a and 1e, the green and red solid lines in Figure 1, which partition PAHs upon emission to primary OM/BC and SOA, respectively, show

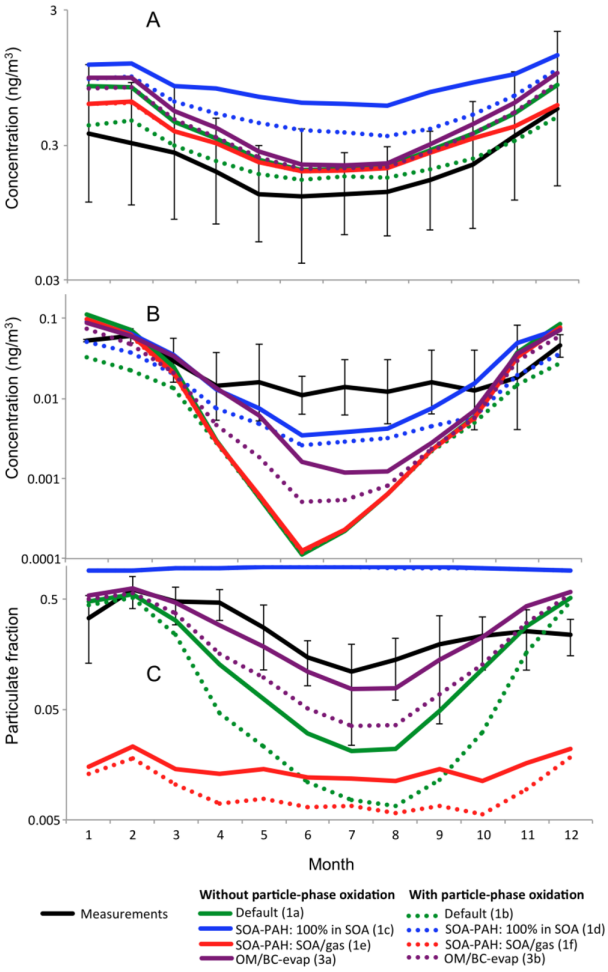

Figure 1. (A) Monthly geometric mean nonurban midlatitude total concentrations, (B) monthly geometric mean Arctic total concentrations, and (C) monthly mean particulate fractions. Results shown are from simulations listed in sections 1 and 3 of Table 1. Results for simulations without (solid lines) and with (dotted lines) particle-phase oxidation are shown. Measured data are for sites in Table S2 in the Supporting Information for 2006–2008. Error bars are ±1 standard deviation of monthly means across sites. Numbers/letters in parentheses correspond to simulation labels from Table 1.

nearly identical results, despite different partitioning behaviors during transport.

Comparison with particulate fractions shows that the SOA–PAH configurations under- and overestimate the particulate fraction while the default configuration performs best (Figure 1C). Default simulations (1a and 1b, Table 1) predict particulate fractions closest to measured values and capture the intermonthly trend of higher particulate fractions in winter versus summer most accurately (green lines, Figure 1C). The particulate fraction is highly overestimated by SOA–PAH simulations with 100% of emissions in SOA, even when particle-phase oxidation is turned on (1c and 1d, Table 1, and solid and dotted blue lines, Figure 1C, respectively). The SOA–PAH 100% entrapment scenario also fails to capture seasonal variation in particulate fraction, predicting higher fractions in summer versus winter, whereas the observed particulate fraction is lowest in summer. In contrast, particulate fractions are severely underestimated in the SOA/gas scenario (simulation 1e; red solid line, Figure 1C), especially when oxidation is implemented (simulation 1f; red dotted line, Figure 1C; >10× lower than mean measured values).

Although concentration and phase distribution results suggest allocating more PAHs to the particulate phase during emission increases LRT, they also imply the two have a complex relationship. This can be observed by comparing 100% in SOA simulations with and without particle-phase oxidation (1c and 1d, Table 1). Implementing particle-phase oxidation does not affect the extreme overestimates of the particulate fraction (blue lines, Figure 1C), but causes notable decreases in concentrations (blue lines, Figure 1A,B). That is, nearly identical particle-phase fractions exhibit different LRT results. Another example is seen when default simulations are compared to SOA/gas emissions scenario simulations (1a and 1b to 1e and 1f, respectively). Simulated particulate fractions vary dramatically between these two configurations (green and red lines, Figure 1C), but predicted total concentrations are very similar (green and red lines, Figure 1A,B). Thus, different particle-phase fractions result in similar total LRT. This complex relationship between phase distribution and total PAH transport has been noted in other PAH modeling studies comparing different partitioning parametrizations.[16] Thus, our results suggest the amount of PAH partitioning to particles cannot alone be used to predict LRT potential.

Arctic particulate fractions from different simulations (Figure S5, Supporting Information) have distinctly different seasonal patterns. We do not compare these to observations, however, as Arctic sampling requires high airflow rates and long sampling periods, which can cause phase resolution artifacts. Similar to midlatitude results, 100% in SOA simulations (1d and 1e) produce the highest particulate fractions (blue lines, Figure S5), though the overall particulate fraction is smaller in the Arctic than at midlatitudes. The particulate fraction for SOA–PAH simulations (blue and red lines) are maximum in summer, while default simulations (green lines) are minimum in summer. While data to constrain seasonal variations in the Arctic particulate fraction have methodological limitations, as noted above, Sofowote et al.[40] found that the pyrene Arctic particulate fraction was maximum in summer and minimum in winter, opposite the results found in the midlatitudes. Sofowote et al. attributed the summer maximum to a shift to local emissions sources (not included in our model emissions). However, this nevertheless suggests SOA–PAH simulations capture the seasonal trend in Arctic particulate fraction better than default simulations.

Effect of Factors Other Than Partitioning. Sensitivity simulations suggest interaction with primary aerosols rather than SOA is more important than the influence of wet deposition efficiency or spatiotemporal variation in OH concentrations for matching observed phase distributions. Figure 2 shows the results of this sensitivity simulation

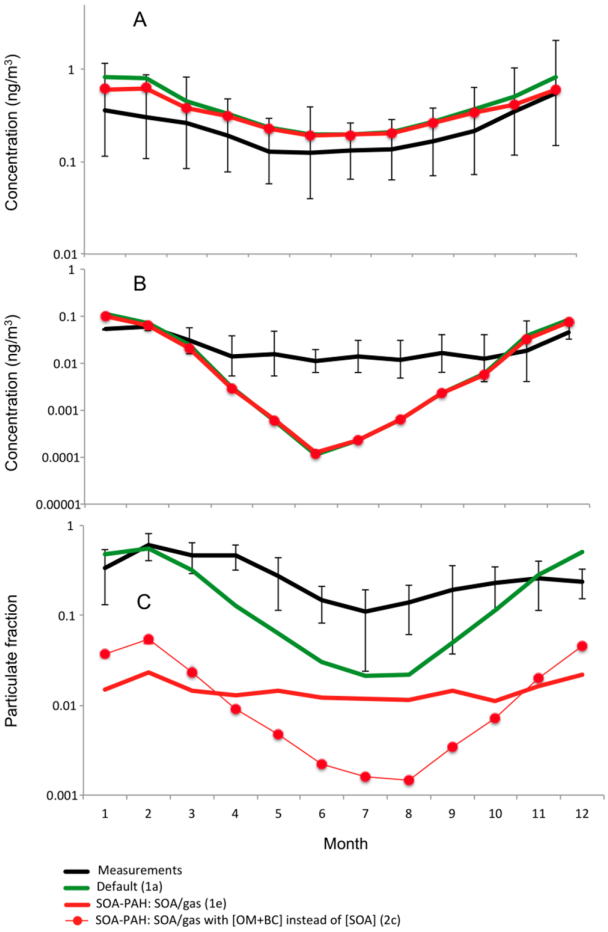

Figure 2. (A) Monthly geometric mean nonurban midlatitude total concentrations, (B) monthly geometric mean Arctic total concentrations, and (C) monthly mean particulate fractions for sensitivity simulations. Simulations did not include particle-phase oxidation, and SOA–PAH model simulations were conducted with 20% evaporation by 24 h. Numbers/letters in parentheses correspond to simulation labels from Table 1.

(simulation 2c, Table 1) compared with observations. Also shown for comparison are default and SOA/gas results for simulations without particle-phase oxidation (i.e., simulations 1a and 1e from Table 1; solid green and red lines from Figure 1). Results of the other two sensitivity simulations are shown (Figure S6) and discussed in the Supporting Information.

Substituting primary OM/BC concentrations for SOA (red line with circles) causes very little change in total concentration (<1% increase in both the midlatitudes and Arctic; Figure 2A,B), but there is an average increase (17%) in particulate fraction (Figure 2C), which better matches observations. More important, the seasonal pattern of particulate fraction in the

dx.doi.org/10.1021/es405219r | Environ. Sci. Technol. 2014, 48, 3293–3302

primary OM/BC concentration sensitivity simulation better matches observations. This is consistent with seasonal trends for aerosols: SOA tends to be higher in summer because emissions correlate with temperature, while primary carbonaceous aerosols often peak in winter because of burning for heat. This suggests interaction with primary aerosols rather than SOA is what drives the better match to observed phase distributions in the default simulation. We note that the addition of greater sources of anthropogenically controlled SOA to OA models has been recommended in the past,[35] and it is possible that anthropogenically controlled SOA could exert similar controls on PAH LRT as primary aerosols. We discuss the potential influence of including these sources[34,35] below.

Assessing the Role of Instantaneous Equilibrium Partitioning versus Aerosol Type. The OM/BC-evap simulation with no particle-phase oxidation (3a, Table 1; purple lines, Figure 1) agrees better than the default configuration (green lines, Figure 1) with the observed phase distribution (Figure 1C) and Arctic concentrations (Figure 1B). Midlatitude results (Figure 1A) are biased high, however, and there is a significant difference between annual simulated and observed means (p = 0.03; Figure S4, Supporting Information). Turning on particle-phase oxidation (simulation 3b) improves midlatitude seasonal (Figure 1A) and annual concentrations, such that there is no longer a significant difference between annual means (p = 0.07; Figure S4), but the match to remote observations degrades, as does the match to the phase distribution (Figure 1B,C).

The OM/BC-evap configuration substantially increases Arctic particulate fractions compared to the default configuration (e.g., from an annual mean of 0.02 for simulation 1a to 0.4 for simulation 3a) and reverses the seasonal pattern (Figure S5, Supporting Information). The OM/BC-evap configuration produces an Arctic particle-phase maximum in summer consistent with what Sofowote et al.[40] observed for pyrene. Thus, the OM/BC-evap configuration captures midlatitude and remote concentrations and phase distributions simultaneously with the most skill.

DISCUSSION

Role of Black Carbon. Our results demonstrate that trapping PAHs in carbonaceous aerosols upon emission improves agreement between measured and simulated PAH concentrations in remote regions and particle phase distributions, compared to a scheme that uses EqP. Simulations employing SOA as the sole particle phase to which PAHs partition result in PAH particulate fractions that are either too high or too low compared to observations, however, and with the opposite seasonal pattern. In contrast, default simulations with EqP between the gas phase and primary hydrophobic carbonaceous aerosols (OM/BC) closely capture particulate fraction magnitude and seasonal variation as well as midlatitude total concentrations, but underestimate remote concentrations. Thus, we created a configuration ("OM/BC-evap") that explicitly considers adsorption to BC (i.e., with K_{BC}) to test whether the strong sorption to BC versus SOA was the main reason for better particle-phase model−observation agreement with the default configuration (versus EqP). Indeed, simulating entrapment of PAHs by BC and limiting exchange with the gas phase provides the best match to all observations, especially with respect to magnitude and seasonality of the phase distribution. Exchange with the gas phase during transport has only a small influence on the ability to reproduce measurements. Collectively, our results suggest two considerations of primary importance in determining PAH LRT, with a particular emphasis on the role of BC: (1) physicochemical behavior governing initial PAH association with particles (i.e., magnitude of partition coefficients and a particle's ability to sequester/trap PAHs during emission) and (2) particle concentrations close to or within emission sources.

Evidence of BC's importance to PAH LRT can be found in the similarity between simulations distributing PAHs between the gas and aerosol phases upon emission. Default (1a and 1b) and SOA−gas emissions (1e and 1f) scenarios predict remarkably similar concentration results, in both the midlatitudes and Arctic, compared with simulations trapping 100% of PAHs in SOA upon emission (1c and 1d). This suggests that PAH gas−particle distribution upon emission is a key process determining how PAHs transport, and PAHs are much more likely associated with BC versus SOA when emitted. Activities producing the greatest PAH emissions globally are also those producing large quantities of BC,[31,41] namely, combustion of biofuels and fossil fuels. Indeed, there is a large amount of literature demonstrating pyrogenic PAHs and BC (or soot) are coemitted, with strong evidence that PAHs are molecular intermediates in the process of BC formation and growth during combustion.[42] While PAHs also have petrogenic and biogenic sources, globally these are minor compared to pyrogenic sources.[31]

An important role for atmospheric BC is consistent with PAH behavior in aquatic/sediment environments and also with results of other studies of PAH partitioning in the air beyond the D&E study. For example, Arp et al.[43] investigated over 500 measured K_p values for a wide range of SVOCs, including PAHs. Their results indicated that for most neutral SVOCs, the water-insoluble OM fraction of aerosol was a good predictor of K_p. PAHs, however, exhibited anomalous behavior in that measured K_p value s were up to ∼100× higher than predicted, which was attributed to a nonexchangeable fraction associated with BC. Indeed, PAHs were the only SVOCs studied that are coemitted with BC.

Uncertainties. The interpretation of our results is subject to a number of uncertainties. First, we do not account for particle size, relative humidity, or particle heterogeneity. PAHs associated with different particle sizes can deposit differently,[44] while humidity can impact oxidation rates[45,46] and diffusion of PAHs to particle surfaces.[38] Within the GEOS-Chem PAH model, primary carbonaceous aerosols consist solely of hydrophobic OM and BC, when in reality aerosols are only partially comprised of these components and can contain a number of other phases, such as minerals and salts.[42,47] Furthermore, the mixing of OM and BC within a single particle from aging could affect PAH partitioning substantially. For example, OM coatings that develop during transport could either diminish PAH adsorption to BC during transport or trap PAHs already associated with BC. Concentrations of primary carbonaceous aerosols, SOA, and oxidants in the PAH model are subject to the uncertainties of the GEOS-Chem NO_x−O_x−hydrocarbon−aerosol model[24,30,48] with which they were generated.

We extend observations of SOA trapping of pyrene, determined via experiments with SOA generated from α-pinene,[22] to BC in our final OM/BC-evap simulations. Given differences between the formation of SOA and BC, it is likely that pyrene−BC interactions differ considerably from pyrene−α-pinene interactions. The process of SOA formation

itself is largely unknown, with ongoing debate as to whether SOA is a semisolid or liquid and whether it is formed primarily from the oxidation of gas-phase precursors or from previously emitted particles. The degree to which PAHs take part in SOA formation is still largely unknown as well, and extending observations of PAH entrapment in SOA to BC adds yet another layer of uncertainty. We acknowledge that our OM/BC-evap configuration may represent a process for which there is little physical evidence in the atmosphere, but nonetheless, the simulations provide valuable information regarding agreement between observations in midlatitude and remote regions.

Additionally, it is possible that introducing greater sources of "anthropogenically enhanced" SOA into the model could produce a PAH phase distribution similar to what we observe with BC. Spracklen et al.[35] recommended adding ∼100 Tg/yr of anthropogenically controlled SOA to model sources to minimize SOA observation−model discrepancies. Heald et al.[24] did just that with the GEOS-Chem SOA model using simulated aromatic SOA as a proxy for anthropogenically controlled SOA and found dramatically better measurement−model agreement near sources, but overestimates aloft and in remote regions. We note that anthropogenically derived SOA and BC sources are likely correlated, and thus, the improved phase distribution model−measurement agreement seen when PAHs partition primarily to BC might also be observed if simulations are conducted with additional anthropogenically controlled SOA instead.

There are uncertainties in pyrene oxidation rates in both the gas and particle phases beyond the impact of humidity. For example, the gas-phase OH reaction rate constant we use for pyrene has been deduced from the ionization potential[49] rather than empirically determined, and particle-phase oxidation rate constants have been measured for PAHs associated with model substrates such as decanol, graphite, or diesel, rather than ambient particulate matter.[32,50−52] These uncertainties could cause considerable variation in the loss of both the gas and particle phases.

Finally, there are uncertainties in emissions, in both magnitude and spatial/temporal distribution, which could lead to deviations in simulation performance. Sensitivity simulations conducted with ±20% of baseline emissions, however, demonstrate no notable change in phase distribution. This suggests gas−particle distributions depend more strongly on the PAH and particle physicochemical behavior and phase distribution when emitted than the emissions magnitude.

■ ASSOCIATED CONTENT

Supporting Information

Physicochemical constants, measurement station data, model and measurement correlation data, and comparison of previous model version results to those presented here. This material is available free of charge via the Internet at http://pubs.acs.org/.

■ AUTHOR INFORMATION

Corresponding Author

*E-mail: clf@mit.edu. Phone: 617-324-2592. Fax: 617-253-7492.

Notes

The authors declare no competing financial interest.

■ ACKNOWLEDGMENTS

This work was supported by the MIT Leading Technology and Policy Initiative and the U.S. National Science Foundation Atmospheric Chemistry (Grant 1053658) and Arctic Natural Sciences (Grant 1203526) programs.

■ REFERENCES

(1) Halsall, C. J.; Barrie, L. A.; Fellin, P.; Muir, D. G. C.; Billeck, B. N.; Lockhart, L.; Rovinsky, F.; Kononov, E.; Pastukhov, B. Spatial and temporal variation of polycyclic aromatic hydrocarbons in the Arctic atmosphere. *Environ. Sci. Technol.* **1997**, *31*, 3593−3599.

(2) Wang, R.; Tao, S.; Wang, B.; Yang, Y.; Lang, C.; Zhang, Y.; Hu, J.; Ma, J.; Hung, H. Sources and pathways of polycyclic aromatic hydrocarbons transported to Alert, the Canadian High Arctic. *Environ. Sci. Technol.* **2010**, *44*, 1017−1022.

(3) Lohmann, R.; Lammel, G. Adsorptive and absorptive contributions to the gas-particle partitioning of polycyclic aromatic hydrocarbons: State of knowledge and recommended parametrization for modeling. *Environ. Sci. Technol.* **2004**, *38*, 3793−3803.

(4) Keyte, I. J.; Harrison, R. M.; Lammel, G. Chemical reactivity and long-range transport potential of polycyclic aromatic hydrocarbons—A review. *Chem. Soc. Rev.* **2013**, *42*, 9333−9391.

(5) Junge, C. E. *Fate of Pollutants in the Air and Water Environment*; Wiley: New York, 1977; Vol. Part *1*, pp 7−25.

(6) Pankow, J. F. Review and comparative-analysis of the theories on partitioning between the gas and aerosol particulate phases in the atmosphere. *Atmos. Environ.* **1987**, *21*, 2275−2283.

(7) Pankow, J. F. An absorption model of gas/particle partitioning of organic compounds in the atmosphere. *Atmos. Environ.* **1994**, *28*, 185−188.

(8) Pankow, J. F. An absorption model of the gas/aerosol partitioning involved in the formation of secondary organic aerosol. *Atmos. Environ.* **1994**, *28*, 189−193.

(9) Finizio, A.; Mackay, D.; Bidleman, T.; Harner, T. Octanol-air partition coefficient as a predictor of partitioning of semi-volatile organic chemicals to aerosols. *Atmos. Environ.* **1997**, *31* (15), 2289−2296.

(10) Harner, T.; Bidleman, T. F. Octanol−air partition coefficient for describing particle/gas partitioning of aromatic compounds in urban air. *Environ. Sci. Technol.* **1998**, *32*, 1494−1502.

(11) Dachs, J.; Eisenreich, S. J. Adsorption onto aerosol soot carbon dominates gas-particle partitioning of polycyclic aromatic hydrocarbons. *Environ. Sci. Technol.* **2000**, *34*, 3690−3697.

(12) Wang, W.; Massey Simonich, S. L.; Wang, W.; Giri, B.; Zhao, J.; Xue; Cao, J.; Lu, X.; Tao, S. Atmospheric polycyclic aromatic hydrocarbon concentrations and gas/particle partitioning at background, rural village and urban sites in the North China Plain. *Atmos. Res.* **2011**, *99*, 197−206.

(13) Lammel, G.; Klánová, J.; Ilić, P.; Kohoutek, J.; Gasić, B.; Kovacić, I.; Skrdlíková, L. Polycyclic aromatic hydrocarbons in air on small spatial and temporal scales—II. Mass size distributions and gas-particle partitioning. *Atmos. Environ.* **2010**, *44*, 5022−5027.

(14) Lammel, G.; Sehili, A. M.; Bond, T. C.; Feichter, J.; Grassl, H. Gas/particle partitioning and global distribution of polycyclic aromatic hydrocarbons—A modelling approach. *Chemosphere* **2009**, *76*, 98−106.

(15) Sehili, A. M.; Lammel, G. Global fate and distribution of polycyclic aromatic hydrocarbons emitted from Europe and Russia. *Atmos. Environ.* **2007**, *41*, 8301−8315.

(16) Galarneau, E.; Makar, P. A.; Zheng, Q.; Narayan, J.; Zhang, J.; Moran, M. D.; Bari, M. A.; Pathela, S.; Chen, A.; Chlumsky, R. PAH concentrations simulated with the AURAMS-PAH chemical transport model over Canada and the USA. *Atmos. Chem. Phys. Discuss.* **2013**, *13*, 18417−18449.

(17) Jonker, M. T. O.; Koelmans, A. A. Sorption of polycyclic aromatic hydrocarbons and polychlorinated biphenyls to soot and soot-like materials in the aqueous environment: Mechanistic considerations. *Environ. Sci. Technol.* **2002**, *36*, 3725−3734.

(18) Gustafsson, O.; Haghseta, F.; Chan, C.; MacFarlane, J.; Gschwend, P. M. Quantification of the dilute sedimentary soot phase: Implications for PAH speciation and bioavailability. *Environ. Sci. Technol.* **1996**, *31* (1), 203−209.
(19) Accardi-Dey, A.; Gschwend, P. M. Assessing the combined roles of natural organic matter and black carbon as sorbents in sediments. *Environ. Sci. Technol.* **2002**, *36* (1), 21−29.
(20) Cornelissen, G.; Gustafsson, O.; Bucheli, T. D.; Jonker, M. T. O.; Koelmans, A. A.; Van Noort, P. C. M. Extensive sorption of organic compounds to black carbon, coal, and kerogen in sediments and soils: Mechanisms and consequences for distribution, bioaccumulation, and biodegradation. *Environ. Sci. Technol.* **2005**, *39* (18), 6881−6895.
(21) Primbs, T.; Piekarz, A.; Wilson, G.; Schmedding, D.; Higginbotham, C.; Field, J.; Simonich, S. M. Influence of Asian and western United States urban areas and fires on the atmospheric transport of polycyclic aromatic hydrocarbons, polychlorinated biphenyls, and fluorotelomer alcohols in the western United States. *Environ. Sci. Technol.* **2008**, *42*, 6385−6391.
(22) Zelenyuk, A.; Imre, D.; Beranek, J.; Abramson, E. H.; Wilson, J.; Shrivastava, M. Synergy between secondary organic aerosols and long-range transport of polycyclic aromatic hydrocarbons. *Environ. Sci. Technol.* **2012**, *46*, 12459−12466.
(23) Robinson, A. L.; Donahue, N. M.; Shrivastava, M. K.; Weitkamp, E. A.; Sage, A. M.; Grieshop, A. P.; Lane, T. E.; Pierce, J. R.; Pandis, S. N. Rethinking organic aerosols: Semivolatile emissions and photochemical aging. *Science* **2007**, *315* (5816), 1259−1262.
(24) Heald, C. L.; Coe, H.; Jimenez, J. L.; Weber, R. J.; Bahreini, R.; Middlebrook, A. M.; Russell, L. M.; Jolleys, M.; Fu, T.-M.; Allan, J. D.; Bower, K. N.; Capes, G.; Crosier, J.; Morgan, W. T.; Robinson, N. H.; Williams, P. I.; Cubison, M. J.; DeCarlo, P. F.; Dunlea, E. J. Exploring the vertical profile of atmospheric organic aerosol: Comparing 17 aircraft field campaigns with a global model. *Atmos. Chem. Phys.* **2011**, *11*, 12673−12696.
(25) Shakya, K. M.; Griffin, R. J. Secondary organic aerosol from photooxidation of polycyclic aromatic hydrocarbons. *Environ. Sci. Technol.* **2010**, *44*, 8134−8139.
(26) Pye, H. O. T.; Pouliot, G. A. Modeling the role of alkanes, polycyclic aromatic hydrocarbons, and their oligomers in secondary organic aerosol formation. *Environ. Sci. Technol.* **2012**, *46*, 6041−6047.
(27) Friedman, C. L.; Selin, N. E. Long-range atmospheric transport of polycyclic aromatic hydrocarbons: A global 3-D model analysis including evaluation of Arctic sources. *Environ. Sci. Technol.* **2012**, *46*, 9501−9510.
(28) Friedman, C. L.; Selin, N. E. Climate change and emissions impacts on atmospheric PAH transport to the Arctic. *Environ. Sci. Technol.* **2014**, *48*, 429−437.
(29) Zhang, Q.; Worsnop, D. R.; Canagaratna, M. R.; Jimenez, J. L. Hydrocarbon-like and oxygenated organic aerosols in Pittsburgh: Insights into sources and processes of organic aerosols. *Atmos. Chem. Phys.* **2005**, *5*, 3289−3311.
(30) Park, R. J.; Jacob, D. J.; Chin, M.; Martin, R. V. Sources of carbonaceous aerosols over the United States and implications for natural visibility. *J. Geophys. Res.* **2003**, *108* (D12), 4355.
(31) Zhang, Y.; Tao, S. Global atmospheric emission inventory of polycyclic aromatic hydrocarbons (PAHs) for 2004. *Atmos. Environ.* **2009**, *43*, 812−819.
(32) Liu, C.; Zhang, P.; Yang, B.; Wang, Y. X.; Shu, J. Kinetic studies of heterogeneous reactions of polycyclic aromatic hydrocarbon aerosols with NO_3 radicals. *Environ. Sci. Technol.* **2012**, *46*, 7575−7580.
(33) Wainwright, C. D.; Pierce, J. R.; Liggio, J.; Strawbridge, K. B.; Macdonald, A. M.; Leaitch, R. W. The effect of model spatial resolution on secondary organic aerosol predictions: A case study at Whistler, BC, Canada. *Atmos. Chem. Phys.* **2012**, *12*, 10911−10923.
(34) D'Andrea, S. D.; Hakkinen, S. A. K.; Westervelt, D. M.; Kuang, C.; Levin, E. J. T.; Leaitch, W. R.; Spracklen, D. V.; Riipinen, I.; Pierce, J. R. Understanding and constraining global secondary organic aerosol amount and size-resolved condensational behavior. *Atmos. Chem. Phys. Discuss.* **2013**, *13*, 18969−19007.
(35) Spracklen, D. V.; Jimenez, J. L.; Carslaw, K. S.; Worsnop, D. R.; Evans, M. J.; Mann, G. W.; Zhang, Q.; Canagaratna, M. R.; Allan, J.; Coe, H.; McFiggans, G.; Rap, A.; Forster, P. Aerosol mass spectrometer constraint on the global secondary organic aerosol budget. *Atmos. Chem. Phys.* **2011**, *11*, 12109−12136.
(36) Chung, S. H.; Seinfeld, J. H. Global distribution and climate forcing of carbonaceous aerosols. *J. Geophys. Res.: Atmos.* **2002**, *107*, 4407.
(37) Wesely, M. L. Parameterization of surface resistances to gaseous dry deposition in regional-scale numerical models. *Atmos. Environ.* **1989**, *23*, 1293−1304.
(38) Shiraiwa, M.; Ammann, M.; Koop, T.; Pöschl, U. Gas uptake and chemical aging of semisolic organic aerosol particles. *Proc. Natl. Acad. Sci. U.S.A.* **2011**, *108*, 11003−11008.
(39) Halsall, C. J.; Sweetman, A. J.; Barrie, L. A.; Jones, K. C. Modelling the behaviour of PAHs during atmospheric transport from the UK to the Arctic. *Atmos. Environ.* **2001**, *35*, 255−267.
(40) Sofowote, U. M.; Hung, H.; Rastogi, A. K.; Westgate, J. N.; Su, Y.; Sverko, E.; D'Sa, I.; Roach, P.; Fellin, P.; McCarry, B. E. The gas/particle partitioning of polycyclic aromatic hydrocarbons collected at a sub-Arctic site in Canada. *Atmos. Environ.* **2010**, *44*, 4919−4926.
(41) Bond, T. C.; Bhardwaj, E.; Dong, R.; Jogani, R.; Jung, S.; Roden, C.; Streets, D. G.; Trautmann, N. M. Historical emissions of black and organic carbon aerosol from energy-related combustion, 1850−2000. *Global Biogeochem. Cycles* **2007**, *21*, GB2018.
(42) Seinfeld, J. H.; Pandis, S. N. *Atmospheric Chemistry and Physics*, 2nd ed.; John Wiley & Sons, Inc.: Hoboken, NJ, 2006.
(43) Arp, H. P. H.; Schwarzenbach, R. P.; Goss, K.-U. Ambient gas/particle partitioning. 2: The influence of particle source and temperature on sorption to dry terrestrial aerosols. *Environ. Sci. Technol.* **2008**, *42*, 5951−5957.
(44) Kaupp, H.; McLachlan, M. S. Atmospheric particle size distributions of polychlorinated dibenzo-*p*-dioxins and dibenzofurans (PCDD/Fs) and polycyclic aromatic hydrocarbons (PAHs) and their implications for wet and dry deposition. *Atmos. Environ.* **1998**, *33*, 85−95.
(45) Shiraiwa, M.; Garland, R. M.; Pöschl, U. Kinetic double-layer model of aerosol surface chemistry and gas-particle interactions (K2-SURF): Degradation of polycyclic aromatic hydrocarbons exposed to O_3, NO_2, H_2O, OH and NO_3. *Atmos. Chem. Phys.* **2009**, *9*, 9571−9586.
(46) Pöschl, U.; Letzel, T.; Schauer, C.; Niessner, R. Interaction of ozone and water vapor with spark discharge soot aerosol particles coated with benzo[*a*]pyrene: O_3 and H_2O adsportion, benzo[*a*]pyrene degradation, and atmospheric implications. *J. Phys. Chem. A* **2001**, *105*, 4029−4041.
(47) Gotz, C. W.; Scheringer, M.; MacLeod, M.; Roth, C. M.; Hungerbuhler, K. Alternative approaches for modeling gas−particle partitioning of semivolatile organic chemicals: Model development and comparison. *Environ. Sci. Technol.* **2007**, *41*, 1272−1278.
(48) Bey, I.; Jacob, D. J.; Yantosca, R. M.; Logan, J. A.; Field, B.; Fiore, A. M.; Li, Q.; Liu, H. X.; Mickley, L. J.; Schultz, M. Global modeling of tropospheric chemistry with assimilated meteorology: Model description and evaluation. *J. Geophys. Res.* **2001**, *106*, 23073−23096.
(49) United States Environmental Protection Agency. *Estimation Programs Interface Suite for Microsoft Windows*, version 4.10; Washington, DC, 2011.
(50) Kahan, T. F.; Kwamena, N.-O. A.; Donaldson, D. J. Heterogeneous ozonation kinetics of polycyclic aromatic hydrocarbons on organic films. *Atmos. Environ.* **2006**, *40*, 3448−3459.
(51) Esteve, W.; Budzinski, H.; Villenave, E. Relative rate constants for the heterogeneous reactions of OH, NO_2 and NO radicals with polycyclic aromatic hydrocarbons adsorbed on carbonaceous particles. Part 1: PAHs adsorbed on 1−2 μm calibrated graphite particles. *Atmos. Environ.* **2004**, *38*, 6063−6072.

(52) Esteve, W.; Budzinski, H.; Villenave, E. Relative rate constants for the heterogeneous reactions of NO_2 and OH radicals with polycyclic aromatic hydrocarbons adsorbed on carbonaceous particles. Part 2: PAHs adsorbed on diesel particulate exhaust SRM 1650a. *Atmos. Environ.* **2006**, *40*, 201−211.

MIT Joint Program on the Science and Policy of Global Change - REPRINT SERIES

FOR THE COMPLETE LIST OF REPRINT TITLES: http://globalchange.mit.edu/research/publications/reprints

2013-22 Is Small Better? A Comparison of the Effect of Large and Small Dams on Cropland Productivity in South Africa, Blanc, É. and E. Strobl, *The World Bank Economic Review,* doi: 10.1093/wber/lht026 (2013)

2013-23 Probabilistic projections of 21st century climate change over Norther Eurasia, Monier, E., A. Sokolov, A. Schlosser, J. Scott and X. Gao, *Environmental Research Letters,* 8(4): 045008 (2013)

2013-24 Quantifying regional economic impacts of CO2 intenstity targets in China, Zhang, D., S. Rausch, V.J. Karplus and X. Zhang, *Energy Economics,* 40(2013): 687–701 (2013)

2013-25 Toward evaluating the effect of climate change on investments in the water resource sector: insights from the forecast and analysis of hydrological indicators in developing countries, Strzepek, K., M. Jacobsen, B. Boehlert and J. Neumann, *Environmental Research Letters,* 8(4): 044014 (2013)

2013-26 Modeling water resources within the framework of the MIT Integrated Global System Model: IGSM-WRS, Strzepek, K., A. Schlosser, A. Gueneau, X. Gao, É. Blanc, C. Fant, B. Rasheed and H.D. Jacoby, *Journal of Advances in Modeling Earth Systems,* 5(3): 638–653 (2013)

2013-27 Economic and emissions impacts of renewable fuel goals for aviation in the US, Winchester, N., D. McConnachie, C. Wollersheim and I.A. Waitz, *Transportation Research Part A: Policy and Practice,* 58(2013):116–128 (2013)

2013-28 An integrated assessment modeling framework for uncertainty studies in global and regional climate change: the MIT IGSM-CAM (version 1.0), Monier, E., J.R. Scott, A.P. Sokolov, C.E. Forest and C.A. Schlosser, *Geosci. Model Dev.* 6: 2063–2085 (2013)

2013-29 Characterization of the wind power resource in Europe and its intermittency, Cosseron, A., U.B. Gunturu and C.A. Schlosser, *Energy Procedia,* 40(2013): 58–66 (2013)

2013-30 Climate Change and Emissions Impacts on Atmospheric PAH Transport to the Arctic, Friedman, C.L., Y. Zhang and N.E. Selin, *Environmental Science & Technology,* online first, doi: 10.1021/es403098w (2013)

2013-31 Cost Concepts for Climate Change Mitigation, Paltsev, S. and P. Capros, *Climate Change Economics,* 4(Suppl.1): 1340003 (2013)

2013-32 Insights and issues with simulating terrestrial DOC loading of Arctic river networks, Kicklighter, D.W., D.J. Hayes, J.W. McClelland, B.J. Peterson, A.D. McGuire and J.M. Melillo, *Ecological Applications,* 23(8): 1817–1836 (2013)

2013-33 A Contemporary Carbon Balance for the Northeast Region of the United States, Lu X., D.W. Kicklighter, J.M. Melillo, P. Yang, B. Rosenzweig, C.J. Vörösmarty, B. Gross and R.J. Stewart, *Environmental Science & Technology,* 47(3): 13230–13238 (2013)

2013-34 European-Led Climate Policy versus Global Mitigation Action: Implications on Trade, Technology, and Energy, De Cian, E., I. Keppo, J. Bollen, S. Carrara, H. Förster, M. Hübler, A. Kanudia, S. Paltsev, R.D. Sands and K. Schumacher, *Climate Change Economics,* 4(Suppl. 1): 1340002 (2013)

2013-35 Beyond 2020—Strategies and Costs for Transforming the European Energy System, Knopf, B., Y.-H.H. Chen, E. De Cian, H. Förster, A. Kanudia, I. Karkatsouli, I. Keppo, T. Koljonen, K. Schumacher, D.P. van Vuuren, *Climate Change Economics,* 4(Suppl. 1): 1340001 (2013)

2013-36 Estimating regional methane surface fluxes: the relative importance of surface and GOSAT mole fraction measurements, Fraser, B., P.I. Palmer, L. Feng, H. Boesch, A. Cogan, R. Parker, E.J. Dlugokencky, P.J. Fraser, P.B. Krummel, R.L. Langenfelds, S. O'Doherty, R.G. Prinn, L.P. Steele, M. van der Schoot and R.F. Weiss, *Atmospheric Chemistry and Physics,* 13: 5697–5713 (2013)

2013-37 The variability of methane, nitrous oxide and sulfur hexaflouride in Northeast India, Ganesan, A.L., A. Chatterjee, R.G. Prinn, C.M. Harth, P.K. Salameh, A.J. Manning, B.D. Hall, J. Mühle, L.K. Meredith, R.F. Weiss, S. O'Doherty and D. Young, *Atmospheric Chemistry and Physics,* 13: 10633–10644 (2013)

2013-38 Integrated economic and climate projections for impact assessment, Paltsev, S., E. Monier, J. Scott, A. Sokolov and J.M. Reilly, *Climatic Change*, October 2013, doi: 10.1007/s10584-013-0892-3 (2013)

2013-39 Fiscal consolidation and climate policy: An overlapping generations perspective, Rausch, S., *Energy Economics,* 40(Supplement 1): S134–S148 (2013)

2014-1 Estimating a global black carbon emissions using a top-down Kalman Filter approach, Cohen, J.B. and C. Wang, *Journal of Geophysical Research—Atmospheres,* 119: 1–17, doi: 10.1002/2013JD019912 (2014)

2014-2 Air quality resolution for health impact assessment: influence of regional characteristics, Thompson, T.M., R.K. Saari and N.E. Selin, *Atmospheric Chemistry and Physics,* 14: 969–978, doi: 10.5194/acp-14-969-2014 (2014)

2014-3 Climate change impacts on extreme events in the United States: an uncertainty analysis, Monier, E. and X. Gao, *Climatic Change,* doi: 10.1007/s10584-013-1048-1 (2014)

2014-4 Will economic restructuring in China reduce trade-embodied CO_2 emissions? Qi, T., N. Winchester, V.J. Karplus, X. Zhang, *Energy Economics,* 42(March): 204–212 (2014)

2014-5 Assessing the Influence of Secondary Organic versus Primary Carbonaceous Aerosols on Long-Range Atmospheric Polycyclic Aromatic Hydrocarbon Transport, Friedman, C.L., J.R. Pierce and N.E. Selin, *Environmental Science and Technology,* 48(6): 3293–3302 (2014)

For limited quantities, Joint Program Reprints are available free of charge. Contact the Joint Program Office to order.

MIT Joint Program on
The Science and Policy of Global Change
Massachusetts Institute of Technology
77 Massachusetts Avenue, E19-411
Cambridge, MA 02139
USA